Наносистеми, наноматеріали, нанотехнології
Nanosystems, Nanomaterials, Nanotechnologies
2010, т. 8, № 3, сс. 663–673

PACS numbers: 61.72.Hh, 76.30.-v, 78.55.Et, 78.67.Bf, 78.67.Tf, 82.35.Np, 82.80.Ej

Properties of ZnO:Mn Nanoparticles Immobilized in Polyethylene Matrix

G. V. Lashkarev, P. V. Demydiuk, G. Yu. Yurkov*, O. I. Dmitriev, O. I. Bykov, L. I. Klochkov, Yu. P. Pyratinskiy**, E. I. Slynko, A. G. Khandozhko***, O. V. Popkov*, N. A. Taratanov*

I. M. Frantsevych Institute for Problems of Materials Science, N.A.S. of Ukraine,
3, Krzhyzhanovsky Str.,
03142 Kyyiv, Ukraine
**A. A. Baikov Institute of Metallurgy and Materials Science of RAS,*
49, Leninsky Prospekt,
119991 Moscow, Russia
***Institute of Physics, N.A.S. of Ukraine,*
46, Prospekt Nauky,
03650 Kyyiv, Ukraine
****Yuriy Fedkovych Chernivtsi National University,*
2, Kotsyubynsky Str.,
58012 Chernivtsi, Ukraine

ZnO:Mn nanoparticles (of 3–5 nm) immobilized in polyethylene matrix are synthesized. The samples with different content of the manganese (5%, 10%, and 20% of initial solution of Mn and Zn precursors) are investigated by means of ESR, PL, and XRD. Thus, the behaviour of the Mn impurities in ZnO is studied. As revealed, the most of the manganese in ZnO forms the second undetermined phase MnO_x or substitute zinc in cation sublattice at the surface layer of the nanoparticles. The value of constant of hyperfine structure of Mn is higher than an expected one ($|A| = 89.5 \cdot 10^{-4}$ cm^{-1} that is significantly differ from the constant of hyperfine structure of Mn incorporated into ZnO single crystal ($76 \cdot 10^{-4}$ cm^{-1})). Photoluminescence measurements reveal wide band of emission in green–red region (500–600 nm), with different position of the maximum depending on the manganese content.

Одержано наночастинки ZnO:Mn розмірами 3–5 нм. За допомогою метод ЕПР, рентґеноструктурної аналізи та фотолюмінесценції досліджувалася структура цих наночастинок з різним вмістом мангану: 5%, 10% та 20% масової частки по відношенню до вихідного розчину прекурсорів. Було показано, що переважна кількість мангану формує другу фазу та заміщує цинок у катіонній підґратниці в поверхневому прошарку цих наночастинок. Значення надтонкої структури в ЕПР-дослідженнях виявилися більшими

за очікуване ($|A| = 89{,}5 \cdot 10^{-4}$ см$^{-1}$, що значно відрізняється від довідникових даних константи надтонкої структури для мангану в кристалічній ґратниці ZnO — $76 \cdot 10^{-4}$ см$^{-1}$). Фотолюмінісцентні міряння виявили широку лінію випромінення в зелено-червоній області спектру 500–600 нм з різним положенням максимуму (залежно від типу зразка).

Получены наночастицы Zno:Mn размерами 3–5 нм. С помощью методов ЭПР, рентгеноструктурного анализа и фотолюминесценции исследовалась структура этих наночастиц с разным содержимым марганца: 5%, 10% и 20% массовой части по отношению к исходному раствору прекурсоров. Было показано, что преобладающее количество марганца формирует вторую фазу и замещает цинк в катионной подрешетке в поверхностной прослойке этих наночастиц. Значение сверхтонкой структуры в ЭПР-исследованиях оказались больше ожидаемых ($|A| = 89{,}5 \cdot 10^{-4}$ см$^{-1}$, что значительно отличается от справочных данных константы сверхтонкой структуры для марганца в кристаллической решетке ZnO — $76 \cdot 10^{-4}$ см$^{-1}$). Фотолюминесцентные измерения выявили широкую линию излучения в зелено-красной области спектра 500–600 нм с разным положением максимума (в зависимости от типа образца).

Key words: nanoparticles, ZnO, Mn, photoluminescence, luminescence, ESR.

(Received 10 June, 2010)

1. INTRODUCTION

Onrush of nanotechnology give rise to reconsideration of functional capacity of well-known materials. In particular, many papers have been dedicated to the research on nanosized systems that are based on zinc oxide.

ZnO is a direct wide-gap (3.37 eV) semiconductor with extremely high exciton binding energy (60 meV). In addition, it is nonexpensive, nontoxic and resistive to the high-energy radiation [1]. These features should create prerequisites for ZnO to be applied in crystalline phosphors as work medium for luminescent centres. Quantitative characteristics of such optical system are altered with transition to nanoscale as a result of profound influence of confinement effects and surface states. The former is based on effect of surface restriction that in turn acts as a potential barrier with endless walls.

As a result, confinement effect leads to increasing of band gap, binding energy of exciton and overlapping of electron–hole wave functions. Each mentioned effect makes its positive contribution to quantum efficiency of the crystalline phosphors what consists in increasing of oscillator strength of band-to-band transition, lifetime of excitons and probability of their interaction with luminescent centres [2].

In order to study such a system, ZnO:Mn^{2+} nanoparticles (NP) immobilized in polyethylene matrix (hereafter *samples*) were synthesized. Manganese is expected to be centre of yellow–green lumines-

cence (~ 580 nm) due to $^4T_1(G)$–$^6A_1$ transition in crystal field of hexagonal symmetry [3] (*e.g.*, ZnS). Moreover, orbital and spin quantum numbers of Mn^{2+} in ground state are LQ0 and $S = 5/2$. Therefore it is also proper element for probing of local surroundings in the host by means of ESR (Mn^{2+} has six lines of hyperfine structure). That is very important upon studying of doped nanoparticles.

As for the synthesis process, the mixture of precursors containing Zn^{2+} and Mn^{2+} ions was introduced into the solution of polyethylene in hydrocarbon oil. Thus, separated particles were protected from agglomeration and atmospheric impact. It was also observed that behaviour of the NP had been correlated by option of zinc and manganese precursors. Therefore, influence of mixtures of precursors $Zn(NO_3)_2$ with $Mn(NO_3)_2$ and $Zn(CH_3COO)_2$ with $Mn(CH_3COO)_2$ on the NP properties was studied.

2. EXPERIMENT

2.1. Synthesis

Investigated NPs were synthesized in compliance with the methodology that was described elsewhere [4, 5]. A water solution of Zn and Mn precursors with the concentration varying from 0.05 to 0.06 mol/l was prepared. LDPE (low-density polyethylene) was dissolved in mineral oil in argon atmosphere using intensive stirring and heating. A solution of precursors was being introduced dropwise into the reaction mass for 24 hours at 250°C. Throughout a synthesis, gaseous products of the reaction and residual water were removed from the reaction vessel by an argon stream. Afterwards, a reaction mass (polymer-nanoparticles–oil) was stirred at a proper temperature for 40 minutes with the purpose to complete thermal decomposition of the initial precursors, then cooled down to room temperature and placed into a Soxhlet extractor where residual oil was completely removed.

Two groups of *samples* were prepared. $Zn(NO_3)_2$ with $Mn(NO_3)_2$ and $Zn(CH_3COO)_2$ with $Mn(CH_3COO)_2$ were used as the zinc and manganese precursors for preparation of the first and second groups of samples, respectively. Three types of *samples* containing 5%, 10%, and 20% wt. of Mn in the initial solution of precursors were studied in both groups (see Table 1).

TABLE 1. List of synthesized samples.

Precursor	I group			II group		
	$Zn(NO_3)_2 + Mn(NO_3)_2$			$Zn(CH_3COO)_2 + Mn(CH_3COO)_2$		
Samples	#291	#292	#293	#294	#295	#296
Content of manganese (% Mn)	5%	10%	20%	5%	10%	20%

2.2. Measurement Equipment

X-ray diffraction measurements (XRD) were performed with modified computer-controlled diffractometer DRON-3M equipped with X-ray tube BSV-28, cupper anode ($\lambda = 1.54$ μkm) and nickel filter. Data processing was performed according to the database of standard XRD spectrum value ASTM (American Society of Testing Materials).

The ESR experiments were performed at X band ~ 10 GHz at room temperature and $T = 77$ K.

Photoluminescence (PL) spectra were excited by nitrogen laser (337 nm) and measured at room temperature.

3. RESULTS AND DISCUSSION

Six *samples* were synthesized (see Table 1). The average size of NP was estimated using TEM instrument (Fig. 1) and assigned to be ~ 3–5 nm. Basing on minimum energy principle for surface strain and TEM image (Fig. 1), the NPs are suggested to have sphere-like shape.

The XRD pattern exhibited a wurtzite structure of ZnO (Fig. 2), for both groups of *samples*. Two *samples* with the highest content of manganese (20%) from every of the groups (#3 and #6) and one *sample* #1 (5% Mn) were chosen to compare with one another. As it can be seen from Fig. 2, they have particularly identical XRD spectra that are characterized by six lines of ZnO hexagonal structure and weak unidentified lines with $2\Theta = 38–49°$. According to the ASTM, these unknown lines can be assigned to be compounds of manganese with oxygen. Thus, we could hardly give unambiguous answer what these phases are, so hereinafter they are referred as MnO_x (Manganese–Oxygen).

A comparative analysis of XRD spectra for #1, #3, and #6 was performed. To reveal difference between these *samples*, two parameters for

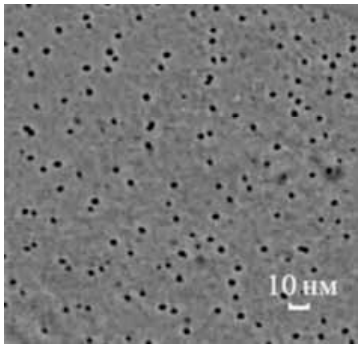

Fig. 1. TEM image of ZnO:Mn nanoparticles. The average size of the NP is 3–5 nm.

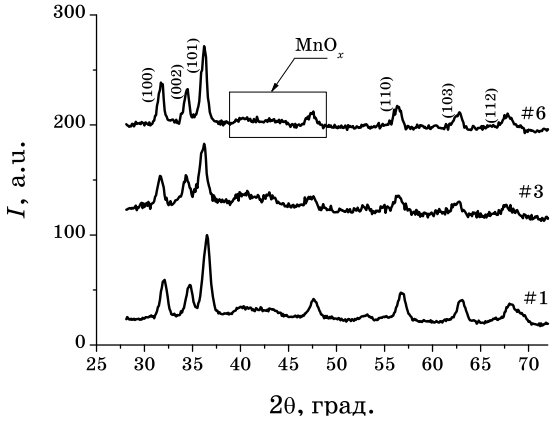

Fig. 2. XRD spectrum for *samples* #1, #3, #6.

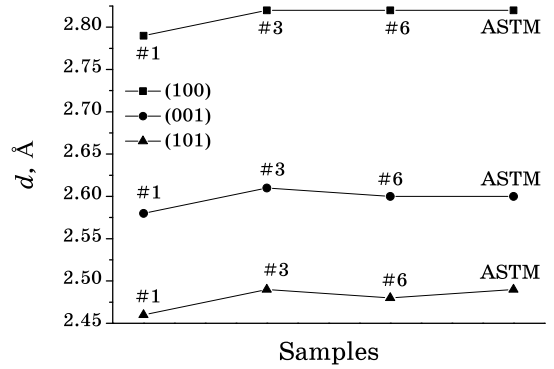

Fig. 3. Comparative values of interplanar spacing of *samples* #1,#3, #6 and corresponding ASTM value for three different directions.

each spectrum were estimated. The first parameter is an interplanar spacing of crystalline structures calculated by Bragg's equation (Fig. 3):

$$d = \frac{\lambda}{2\sin\theta}. \tag{1}$$

Second parameter is a relative size of coherent scattering region (CSR), calculated on the basis of Debye–Scherrer equation (Table 2):

$$\Lambda \cong \frac{\lambda}{\mathrm{FWHM}\cdot\cos\theta}. \tag{2}$$

This parameter in contrast to the first one depends on FWHM of the XRD spectra lines and is used to estimate comparative characteristic (not absolute) of coherent scattering region of the nanoparticles.

TABLE 2. Relative value of coherent scattering region of three samples #1, #3, and #6 calculated by Eq. (2).

Coherent Scattering Region (Å)	ZnO (100)	ZnO (002)	ZnO (101)
#1	2.07	2.46	2.02
#3	2.25	2.25	2.16
#6	2.49	3.30	2.49

FWHM have been calculated as full width at half maximum on Gauss curve that approximate the XRD spectrum lines.

In both equations (1) and (2), the notations θ and λ stand for the scattering angle and wavelength of 1.54 μm, respectively.

One can see (Fig. 3) that interplanar spacing of crystalline lattice of ZnO nanoparticles in *sample* #1 (5% Mn) are slightly shifted to the lower values in comparison with the ones for #3, #6, and ASTM. Such behaviour can be explained if we take into account an effect of surface tension on periods of the crystalline structure. For nanoparticles where surface-to-volume ratio is high, crystalline structure is strongly affected by surface tension that results in decreasing of the periods of the crystalline lattice. In addition, the dimension of the coherent scattering region (Table 2) for these three *samples* has similar dependence, except for the (002) case. Thus, basing on these facts, we can assume that average size of NPs ZnO:Mn #1 is smaller than NP #3 and #6.

3.1. ESR Measurements

Due to half-filled d shell ($3d^5$) with spin $S = 5/2$, angular momentum $L = 0$ and nucleus spin $I = 5/2$, the resonance of an isolated Mn^{2+} ion located substitutionally on a Zn site in hexagonal ZnO is described by the spin Hamiltonian:

$$H = g\mu_B HS + A_{ij}S_iI_j + D_{ij}S_iS_j\,. \qquad (3)$$

At low concentration (< 0.1%) of Mn in doped ZnO single crystals, an isotropic Zeeman (the first term in Eq. (3)) and hyperfine interaction (the second term in Eq. (3)) were observed ($g = 2.0016$, $|A| = 76{\cdot}10^{-4}$ cm^{-1}) together with an axial fine structure splitting ($D = 216.9{\cdot}10^{-4}$ cm^{-1}) [6].

In the case of randomly oriented nanocrystals, anisotropic contributions are washed out and one can expect a six line spectrum with a hyperfine splitting (hereafter, HFS) of about $76{\cdot}10^{-4}$ cm^{-1} from isolated Mn^{2+} incorporated in the ZnO single crystal.

ESR measurements were used to investigate behaviour of Mn^{2+} in the host material ZnO. ESR spectrums for all six *samples* are given in

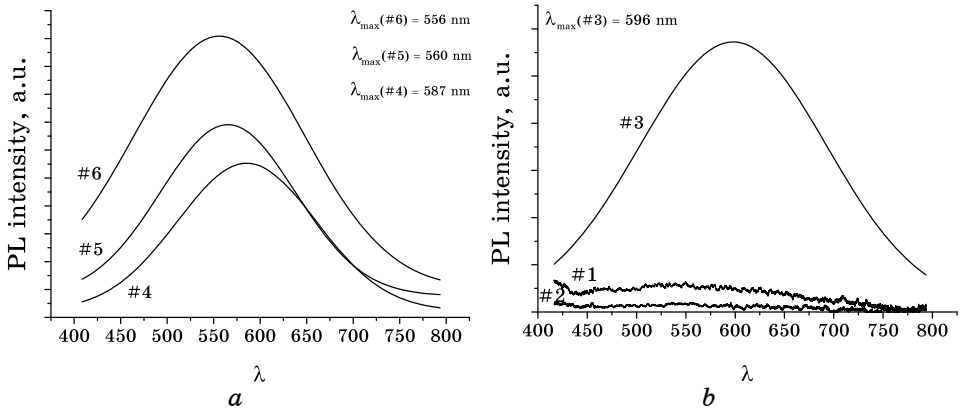

Fig. 4. PL spectra for *samples* (*a*) #1–#3 and (*b*) #4–#6.

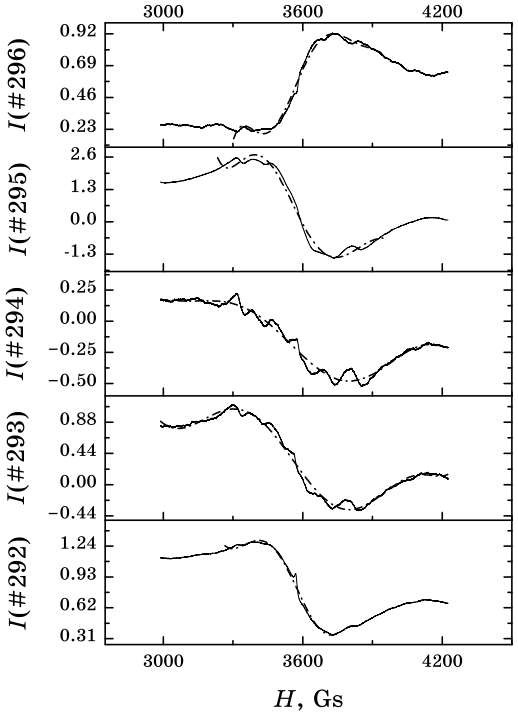

Fig. 5. ESR spectrum for *samples* ##292–296 at $T = 300$ K.

Fig. 5 and Fig. 6. According to these measurements, three spectrum patterns can be highlighted.

S1—broad background line ($g = 1.999$) that inhere for all ESR spectrums (dash-dotted lines in Fig. 5) is related to the exchange and di-

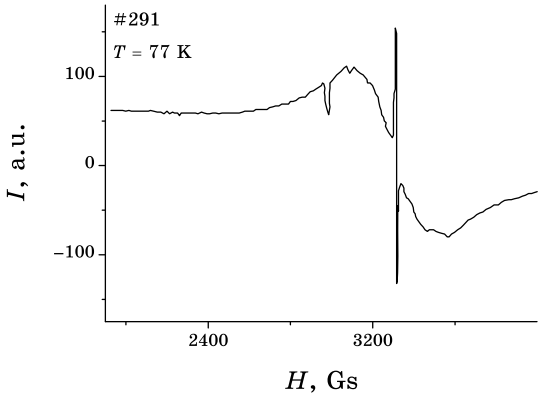

Fig. 6. ESR spectrum for #291 at $T = 77$ K.

TABLE 3. Comparative table of constants of hyperfine structure for Mn in local octahedral and tetrahedral surroundings.

Octahedral surrounding		Tetrahedral surrounding	
	A(10^{-3} cm^{-1})		A(10^{-3} cm^{-1})
ZnF_2	9.6	ZnO	7.4
NaCl	8.2	CdS	6.48
KCl	8.86	CdTe	5.51
NaF	9.1	Al_2O_3	7.5
AgCl	8.1	ZnS	6.4
$SrCl_2$	9.7		

pole–dipole interaction of Mn between nearby magnetic centres. Thus, this line can be attributed to the unknown phase MnO_x (Fig. 2).

S2—six lined hyperfine structure with constant of HFS (CHFS) $A = 94 \cdot 10^{-4}$ cm^{-1} and $g = 2.001$ are related to the isolated Mn in ZnO lattice.

In hexagonal ZnO lattice, manganese ions, which substitute Zn^{2+} in the single crystal, undergo the effect of tetrahedral electrostatic field of the surroundings. In such a case, the CHFS of Mn^{2+} is $76 \cdot 10^{-4}$ cm^{-1}, in contrast to observed HFS of Mn in ZnO nanoparticles with considerably higher CHFS ($A = 94 \cdot 10^{-4}$ cm^{-1}).

Similar increasing of CHFS for manganese in hexagonal lattice has been observed earlier in nanopowders CdS, ZnS [7–9], and ZnO [10] synthesized in colloidal solution. Such increasing in these works related to formation of cubic $Zn(OH)_2$ crystalline phase on the surface of the nanoparticles. In this structure, Mn^{2+} can substitute zinc ions in octahedral surrounding of hydroxide groups. However, in our work the synthesis was held under such conditions that exclude formation of any compounds except ZnO and manganese oxides. Thus, explanation of such

value of CHFS can be related to the disturbances of tetrahedral Zn sublattice at the surface layer of ZnO and formation of octahedral surrounding around manganese ions.

This conclusion is based on the fact that CHFS of Mn in tetrahedral surrounding has lower value than in the case of octahedral one (Table 3). As it can be seen from this table, CHFS $A = 94 \cdot 10^{-4}$ cm^{-1} lay in the range of the values for octahedral local environment.

S3—narrow intensive line with $g = 2.001$. The one is absent on (Fig.5) but emerge on the ESR spectrum for #1 at $T = 77$ K (Fig. 6). This line is obviously attributed to electrons localized on the surface defect centres [11].

These three spectra S1, S2 and S3 are more or less detected for investigated *samples* ##1–6. In particular, S1 ESR signal is well observed for whole number of *Samples* that indicate the second phase formation (compound with Mn component) for all of them. In addition, detailed investigations have shown that S3 signal is present in all ESR spectra too, but strongly overlapped with wide S1 signals. Sextet structure S2 is weakly resolved for members of second group (##4–6), but nearly absent for *samples* #1 and #2. The difference between these two groups lays in type of Zn and Mn precursors that are used in chemical synthesis reaction. From this point of view manganese, which is easily oxidized metal, differently acts in nitride and acetate solutions [3]. In the second group of precursors, the Mn oxidation is more inhibited than in nitrides solution. That leads to increasing of second phase formation in the last medium in comparison with the first one. Therefore, one can observe more intensive six lined structure for #4 and #5 than for #1 and #2.

3.2. PL Spectrum

The PL spectrum of bulk ZnO is characterized by two lines. The first one lies in UV region of 350–370 nm and is attributed to the near band-gap exciton recombination PL. The second one, wide band line, lies in green-red region of the visible spectrum (500–600 nm) and caused by intrinsic point defects within zinc oxide that lead to appearing of deep and shallow defects levels in the band gap [12, 13].

At the transition to nanosized objects, the PL spectrum becomes more ambiguous than in the bulk case. Since influence of surface, layer states in such entities are significantly enhanced with decreasing of their size. Thus, it is expected to observe additional lines in the spectrum of nano-ZnO attributed to the surface layer. The lines can be varied depending on the shape of the nanoparticles.

In Figure 4, spectra of nanoparticles ZnO doped with Mn are shown. All *samples* are characterized by UV component (~ 370 nm) that is poor resolved on the UV band of nitrogen laser background (this line is not

shown on the pictures). In addition, wide band in visible region of the spectrum (500–600 nm) is observed too. The significant widening of this line is clearly attributed to wide distribution of the emission spectrum of the individual nanoparticle within any of the *samples*. Characteristic dimensions of these nanoparticles are decreased enough that their shape and dimensions have significant influence on the optical transitions.

For the *samples* #1–2, the intensity of the lines in visible region lies at the noise level. In these nanoparticles, the radiationless transition is dominated. However, as for the *samples* with higher manganese content, there is intensive line of emission centred at the 590 nm (Fig. 4, *a*). Similar picture is observed for Samples #4–6, the *samples* with the highest manganese content show the most intensive line in the visible region (Fig. 4, *b*).

There is not enough information to conclude definitely about origin of these lines, but some assumption can be made. Whereas the band line strongly overlaps region of defect emission that attributed to the native point defects in ZnO [12], we can assume that one of the sources of the green emission is these point defects.

It is also shown by ESR measurement that revealed point defects in the *samples*. Even in the *samples* #1–2 there are low resolved picks in 530 nm. Other sources of the emission are assumed the surface states, which depend on manganese content at the surface layer of the nanoparticles. Absence of the isolate manganese in the *samples* #1–2 is also confirmed by ESR measurements. For other *samples* where isolate manganese was found by ESR, the PL spectra have been observed. Therefore, we can assume that manganese acts as surface agent that in some way activate emission in visible region of the spectrum.

The role of the manganese as surfactant agent, but not luminescence centre is proved by different position of the PL lines for the *Samples* with different manganese contents. However, luminescence of the manganese (580 nm) could not be eliminated.

4. SUMMARY

In this work, nanoparticles ZnO doped with Mn immobilized in polyethylene matrix with average size 3–5 nm were synthesized.

Two different localizations of Mn have been revealed. The first one is localization at the surface layer substituting zinc in cation sublattice ($|A| = 89.5 \cdot 10^{-4}$ cm^{-1} that differs from constant of hyperfine structure for ZnO ($76 \cdot 10^{-4}$ cm^{-1})). The second one is thought to form undefined phase MnO_x with unresolved hyperfine structure and with factor $g = 2.001$.

Under nitrogen laser excitation (337 nm), visible emission in the range 500–600 nm has been observed that is attributed to defect surface states that are predominant in the nanoparticles.

ACKNOWLEDGEMENT

This work was financed by the Russian Foundation for Basic Research (grant nos. 10-08-90421-Укр and 10-03-00466-а) and the grant of the President of the Russian Federation MD-5551.2010.3.

REFERENCES

1. C. Klingshirn, *Phys. Stat. Sol. B*, **9**: 3027 (2007).
2. J. D. Bryan and D. R. Gamelin, *Progress in Inorganic Chemistry*, **54**: 47 (2005).
3. N. S. Norberg, K. R. Kittilstved, J. E. Amonette, R. K. Kukkadapu, D. A. Schwartz, and D. R. Gamelin, *J. Am. Chem. Soc.*, **30**: 9387 (2004).
4. I. D. Kosobudski, N. M. Ushakov, G. Yu. Yurkov, K. V. Zapsis, V. I. Kochubei, D. A. Baranov, I. P. Dotsenko, M. N. Zhuravleva, K. Yu. Ponamareva, and S. P. Gubin, *Inorganic Materials*, **41**: 1330 (2005).
5. S. P. Gubin, Yu. I. Spichkin, G. Yu. Yurkov, A. M. Tishin, *Russian Journal of Inorganic Chemistry*, **47**: 32 (2002).
6. S. A. Altshuler and B. M. Kozjurev, *Electron Paramagnetic Resonanse of the Compounds of the Elements of Transitions Groups* (Moscow: Nauka: 1972).
7. T. K. Kennedy, E. R. Glaser, P. B. Klein, and R. N. Bhargava, *Phys. Rev. B*, **52**: R14356 (1995).
8. P. H. Borse, D. Srinivas, R. F. Shinde, S. K. Date, W. Vogel, and S. K. Kulkarni, *Phys. Rev. B*, **60**: 8659 (1999).
9. G. Counio, S. Esnouf, T. Gacoin, and J.-P. Boilot, *J. Phys. Chem.*, **100**: No. 51: 20021 (1996).
10. H. Zhou, D. M. Hofmann, A. Hofstaetter, and B. K. Meyer, *J. Appl. Phys.*, **94**: (2003).
11. V. N. Shevchuk, D. I. Popovich, Yu. M. Usatenko, R. Ja. Serkiz, O. V. Tsvetova, *Physics and Chemistry of Solid State*, **10**: 289 (2009).
12. Ü. Özgür, Ya. I. Alivov, C. Liu, A. Teke, M. A. Reshchikov, S. Doğan,V. Avrutin, S.-J. Cho, and H. Morkoç, *J. Appl. Phys.*, **98**: 041301 (2005).
13. V. A. Karpina, V. D. Khranovskyy, V. I. Lazorenko, G. V. Lashkarev, I. V. Blonsky, and V. A. Baturin, *A Material for Micro- and Optoelectronic Applications*, **194**: 59 (2005).